Version of Record: https://www.sciencedirect.com/science/article/pii/S2405896320326999
Manuscript_c971ea7394ac69d1ca8c8287e0689c3e

A new dynamical repulsive fractional potential for UAVs in 3D dynamical environments

Kendric Ruiz[*,**] **Stéphane Victor**[*] **Pierre Melchior**[*] **Serge Chaumette**[**]

[*] *Université de Bordeaux, CNRS, IMS UMR 5218 , Bordeaux INP/enseirb-matmeca – 351 cours de la Libération, 33405 Talence cedex, France*
(email: firstname.lastname@ims-bordeaux.fr)
[**] *Université de Bordeaux, CNRS, Labri UMR 5800 , Bordeaux INP/enseirb-matmeca – 351 cours de la Libération, 33405 Talence cedex, France*
(email: firstname.lastname@labri.fr)

Abstract: In recent years, applications for drones have increased, from surveillance, exploration, rescue to transport applications. UAVs are more and more autonomous, therefore real-time trajectory planning is necessary and can be achieved with potential fields. A study is proposed to better scale attractive and repulsive forces which has always been problematic when dealing with artificial potential fields. The purpose of this article is to develop a new dynamical fractional potential repulsive field usable in a 3D environment by taking into account the obstacle dynamics (position and speed) and their dangerousness. Obstacle avoidance robustness is guaranteed, both from a safety point of view and from a trajectory optimization point of view. The potential fields are based on the relative position and speed of the drone in relation to the target for the attractive potential field or to the obstacle for the repulsive one.

Keywords: Mobile Robots, Potential Fields, Path Planning, Optimal Trajectories, Dynamical Motion Planning

1. INTRODUCTION

Path planning is used to find a suitable path between two points while avoiding obstacles in the environment. These obstacles can be dynamical or static. The notion of danger is therefore necessary to avoid a type of obstacle in the most harmonious way. Artificial potential field (PF) methods has been extensively studied, see *e.g.* Khatib (1985); Krogh and Thorpe (1986); Sfeir et al. (2011); Receveur et al. (2019). However, most methods are generally adapted for a static environment or do not take into account the type of obstacle (see e.g. Li et al. (2015); Mac et al. (2016)). Ge and Cui (2002) have improved work on artificial potential fields by taking into account the obstacle dynamics. Furthermore, Poty et al. (2004) and Metoui et al. (2009) have interpreted the attractive field as a control loop ensuring stability degree robustness of the trajectory towards mass variations of the ego-vehicle and disturbances by taking into account the position and speed of the target as defined by Ge and Cui (see Fig. 1). Moreover, a novel interpretation of robust control is proposed in Receveur et al. (2019) for autonomous vehicles.

The goal of this article is to present a new potential repulsive field adapted to a dynamical 3D environment that ensures the robustness of the trajectory. Potential fields are well adapted for drone applications because the holonomic model of a drone can be identified by a point mass. The PF method allows this mass to be taken into account for both attractive and repulsive fields. The concept of danger will also be a priori taken into account, the obstacles will be considered as known and the method makes it possible to avoid the obstacles with a smoother trajectory according to the obstacle type, in other words, its dangerousness (pedestrian, building, bicycle, car etc.).

In Ge & Cui, no distinction is proposed to differentiate the dangerousness of obstacles. Therefore, Weyl repulsive potential definition has introduced a fractional degree to distinguish obstacles by their dangerousness. It is safer to go nearer a wall than a human. Unfortunately, by gaining on differentiating obstacle danger, the dynamical behaviors of obstacles have been lost. Therefore, a new definition of repulsive field is proposed which takes into account both dangerousness and dynamics of the obstacles. Furthermore, it is often difficult to scale the attractive and repulsive potential forces. A methodology is proposed to efficiently scale them.

The context and the Ge & Cui attractive force is presented in section 2. Section 3 presents the repulsive force background and defines the new dynamical fractional repulsive force. A set of simulation results is presented in section 4, and a conclusion is drawn in section 5.

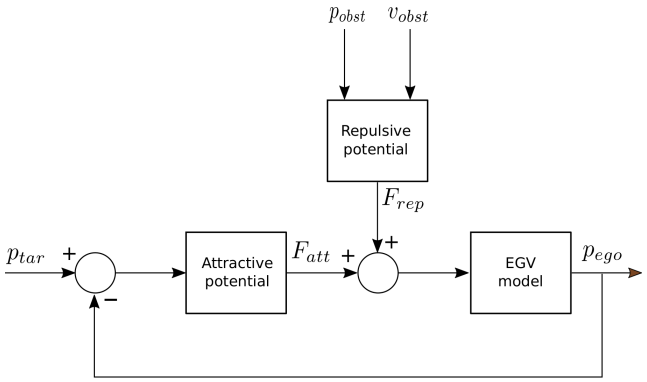

Fig. 1. Dynamical interpretation of Ge and Cui attractive and repulsive forces

2. CONTEXT

During a flight, the UAV can encounter many different obstacles such as pedestrians, birds, trees, which are not necessarily predictable before the UAV takes off. Therefore, a local obstacle avoidance system is proposed when surrounding objects have been detected. Given the detection capacity of the usual sensors (LIDAR, camera), a distance of one hundred meters is considered.

In order to compare our new repulsive PF to classic repulsive fields, the same attractive PF is designed, as presented by Ge and Cui (2002).

2.1 Attractive force background

In Metoui et al. (2009), the Ge and Cui (2002) method has been reinterpreted as a control loop, see Figure 1.

The force presented makes it possible to obtain a real-time trajectory that takes into account the position and speed of the ego-vehicle as well as the target. This virtual attractive force is defined by:

$$F_{att} = \alpha_p \left(\boldsymbol{p}_{tar} - \boldsymbol{p}_{ego}\right) + \alpha_v \left(\boldsymbol{v}_{tar} - \boldsymbol{v}_{ego}\right) \tag{1}$$

where $\boldsymbol{p}_{tar}$ and $\boldsymbol{p}_{ego}$ respectively are the real-time positions of the target and the ego-vehicle (EGV). $\boldsymbol{v}_{tar}$ and $\boldsymbol{v}_{ego}$ respectively are the real-time speeds of the target and the ego-vehicle. α_p and α_v are positive constants that define a lead-phase controller. With the help of this representation as a control loop, it is possible to imagine integrating other types of controllers (see Melchior et al. (2012)). Due to the different obstacles, the forces stemming from the repulsive fields will then be considered as disturbances in the control loop, such as shown in Figure 1.

Equation (1) can be written as:

$$F_{att} = m_{ego}\left(\boldsymbol{a}_{tar} - \boldsymbol{a}_{ego}\right) = \alpha_p \left(\boldsymbol{p}_{tar} - \boldsymbol{p}_{ego}\right) + \alpha_v \frac{d\left(\boldsymbol{p}_{tar} - \boldsymbol{p}_{ego}\right)}{dt}. \tag{2}$$

Introducing the error $e(t) = \boldsymbol{p}_{tar} - \boldsymbol{p}_{ego}$, it then comes:

$$F_{att} = \alpha_p e(t) + \alpha_v \frac{de(t)}{dt}, \tag{3}$$

where $\boldsymbol{a}_{tar}$ and $\boldsymbol{a}_{ego}$ respectively are the real-time acceleration of the target and the ego-vehicle and m_{ego} is the mass of the ego-vehicle.

Under zero initial conditions, the Laplace transform of relation (3) gives:

$$F_{att}(s) = \left(\alpha_p + \alpha_v s\right) E(s), \tag{4}$$

where $E(s)$ is the Laplace transform of $e(t)$. For causality reasons, this proportional derivative (or lead-phase) controller is put under a proper form, namely:

$$\begin{aligned} F_{att}(s) &= C(s)E(s) \\ &= \frac{\alpha_p + \alpha_v s}{1 + \frac{s}{\omega_c}} E(s) = \alpha_p \left(\frac{1 + \frac{\alpha_v}{\alpha_p} s}{1 + \frac{s}{\omega_c}}\right) E(s), \end{aligned} \tag{5}$$

where ω_c is the filter cut-off frequency to make the controller causal. This lead-phase controller $C(s)$ can be rewritten as:

$$C(s) = C_0 \left(\frac{1 + \frac{s}{\omega_b}}{1 + \frac{s}{\omega_h}}\right), \tag{6}$$

where $C_0 = \alpha_p$, $\omega_b = \frac{\alpha_p}{\alpha_v}$, $\omega_h = \omega_c$. The open-loop gain crossover frequency ω_{cg} is directly deduced from the desired time response $tr_{5\%} = \frac{3}{\omega_{cg}}$. With a desired stability given by the phase margin M_φ, the desired lead phase is

$$\phi_m = -\pi + M_\varphi - Arg(G(j\omega_{cg}), \tag{7}$$

where $G(j\omega) = 1/(m_{ego}(j\omega)^2)$ is the EGV transmittance. ϕ_m helps defining the ratio $a = \omega_h/\omega_b$ with

$$a = \frac{1 + sin(\phi_m)}{1 - sin(\phi_m)} \tag{8}$$

and consequently

$$\omega_b = \frac{\omega_u}{\sqrt{a}}$$
$$\omega_h = \omega_u \sqrt{a}.$$

Finally, C_0 is calculated such that the open-loop gain equals one at ω_{cg}:

$$C_0 = \frac{1}{|G(j\omega_{cg}|} \frac{\sqrt{1 + \left(\frac{\omega_{cg}}{\omega_h}\right)^2}}{\sqrt{1 + \left(\frac{\omega_{cg}}{\omega_b}\right)^2}} = \frac{m_{ego}.\omega_{cg}^2}{\sqrt{a}}. \tag{9}$$

For the simulation, $m_{ego} = 1.5$kg, the desired time response is $tr_{5\%} = 3s$, which gives $\omega_{cg} = 1$rad/s. For a stability degree of phase margin $M_\varphi = 60°$, the following parameters are obtained: $\phi_m = 60°$, $a = 13.93$, $\omega_b = 0.27$rad/s, $\omega_h = 3.7$rad/s and $C_0 = 0.4$.

In the following section, the definition of the potential repulsive field is recalled and a new definition is proposed in order to take into account the dynamical aspect of the environment along with the obstacle dangerousness.

3. REPULSIVE POTENTIEL FIELD

3.1 Ge and Cui Repulsive force

As a reminder, this repulsive PF was proposed by Khatib (1985), and is defined as follows:

$$U(\rho) = \begin{cases} \frac{1}{2}\eta \left(\frac{1}{\rho} - \frac{1}{\rho_{min}}\right)^2 & \text{if } \rho \leq \rho min \\ 0 & \text{if } \rho > \rho_{min}, \end{cases} \tag{10}$$

where ρ is the distance between the UAV and the obstacle, ρ_{min} is the shortest safety distance to the obstacle and η is a weighting factor.
From this potential, other definitions have emerged including the one of Ge and Cui (2002), where the speed enables

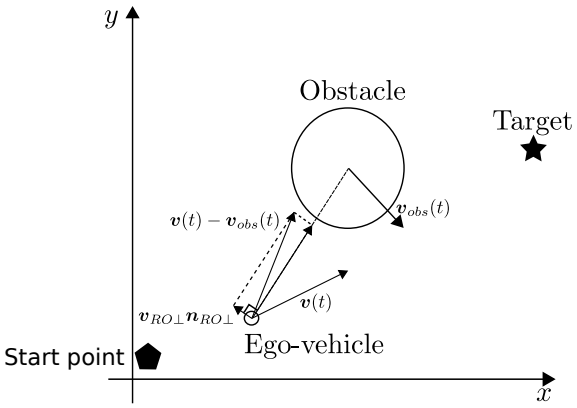

Fig. 2. Representation of the scenario

taking into account the EGV that evolves in a dynamical environment. This PF is defined as follows:

$$U_{rep}(\boldsymbol{p}, \boldsymbol{v}) = \eta \left(\frac{1}{\rho_s(\boldsymbol{p}, \boldsymbol{p}_{obs}) - \rho_m(v_{RO})} - \frac{1}{\rho_{min}} \right), \quad (11)$$

where $\rho_s(\boldsymbol{p}, \boldsymbol{p}_{obs}) = |\boldsymbol{p} - \boldsymbol{p}_{obs}|$ and $\rho_m(v_{RO})$ is defined in (13). As a comparaison, the squared power is removed and the distance ρ is replaced by $\rho_s(\boldsymbol{p}, \boldsymbol{p}_{obs}) - \rho_m(v_{RO})$, an expression that takes into account the relative speed between the EGV and the obstacle. Figure 2 illustrates the methodology in 2D, but this solution also works in 3D.

The relative speed between the robot and the obstacle is defined as:

$$v_{RO}(t) = [\boldsymbol{v}(t) - \boldsymbol{v}_{obs}(t)]^T \boldsymbol{n}_{RO}, \quad (12)$$

where $\boldsymbol{n}_{RO}$ is a unit vector going from the robot to the obstacle. $\boldsymbol{v}(t)$ and $\boldsymbol{v}_{obs}(t)$ respectively are the instantaneous speeds of the robot and the obstacle. Thus, knowing the maximum acceleration a_{max}, it is possible to determine the distance travelled by the robot:

$$\rho_m(v_{RO}) = \frac{v_{RO}^2(t)}{2a_{max}}. \quad (13)$$

From expression (11), the resulting force, corresponding to the negative gradient of the potential, is:

$$\begin{aligned} \boldsymbol{F}_{rep} &= -\nabla U_{rep}(\boldsymbol{p}, \boldsymbol{v}) \\ &= -\nabla_p U_{rep}(\boldsymbol{p}, \boldsymbol{v}) - \nabla_v U_{rep}(\boldsymbol{p}, \boldsymbol{v}) \end{aligned} \quad (14)$$

where

$$\nabla_p U_{rep}(\boldsymbol{p}, \boldsymbol{v}) = \frac{-\eta \left(1 + \frac{v_{RO}}{a_{max}}\right)}{\left(\rho_s(\boldsymbol{p}, \boldsymbol{p}_{obs}) - \rho_m(v_{RO})\right)^2} \boldsymbol{n}_{RO} \quad (15)$$

and

$$\nabla_v U_{rep}(\boldsymbol{p}, \boldsymbol{v}) = \frac{\eta v_{RO} \boldsymbol{v}_{RO\perp} \cdot \boldsymbol{n}_{RO\perp}}{\rho_s(\boldsymbol{p}, \boldsymbol{p}_{obs}) a_{max} \left(\rho_s(\boldsymbol{p}, \boldsymbol{p}_{obs}) - \rho_m(v_{RO})\right)^2} \quad (16)$$

with $v_{RO\perp} = \sqrt{\|\boldsymbol{v}(t) - \boldsymbol{v}_{obs}(t)\|^2 - \|v_{RO}(t)\|^2}$ being the magnitude of the relative velocity between the robot and the obstacle. Note that the vector $v_{RO\perp} \boldsymbol{n}_{RO\perp}$ is perpendicular to the line passing through the robot and the obstacle.

3.2 Repulsive Weyl potential field

Poty et al. (2004) generalized the PF from Weyl's definition. This allows the PF to be defined with an order n

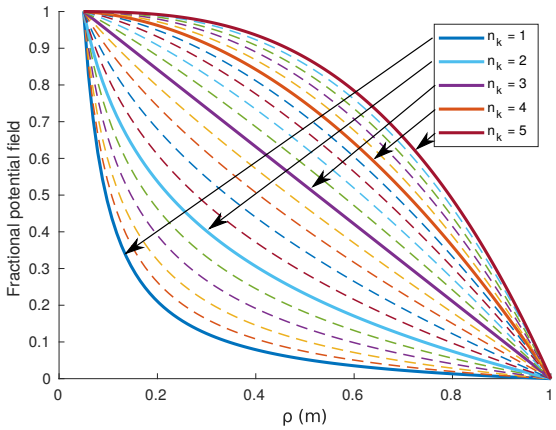

Fig. 3. Influence distance of the normalized fractional potential based on Weyl's definition

that influences the evolution of the field as a function of the distance. This order n is therefore used to adjust the repulsive force according to the obstacle dangerousness. The fractional potential field is defined as follows:

$$U_n^{rep}(\rho) = \begin{cases} \dfrac{\rho^{n-2} - \rho_{max}^{n-2}}{\rho_{min}^{n-2} - \rho_{max}^{n-2}}, & \forall n \in]0;2[\cup]2;+\infty[, \\ & \forall \rho \in [\rho_{min}; \rho_{max}] \\ \dfrac{\ln(\rho_{max}) - \ln(\rho)}{\ln(\rho_{max}) - \ln(\rho_{min})}, & n = 2, \forall \rho \in [\rho_{min}; \rho_{max}] \\ 0, & \forall \rho > \rho_{max} \end{cases} \quad (17)$$

Figure 3 illustrates the Weyl repulsive potential field shape for $\rho_{max} = 1m$ and $\rho_{min} = 0.05m$.

The force represents the gradient of the potential field: the higher the order, the greater the repulsive force at ρ_{max} but on the other hand, the lower its magnitude at ρ_{min}, thus leading to avoid the obstacle as soon as possible. However, if for some reason the obstacle is very close, the repulsive force will not be sufficiently high and a risk of collision is possible. On the contrary, the lower the order, the greater the repulsive force magnitude when getting closer to ρ_{max}, thus allowing smoother path for obstacle avoidance. In Receveur et al. (2019) for a car, a rule associates the value of degree n according to the vulnerability and unpredictability of the obstacle. This rule can be adapted for a UAV.

3.3 Dynamical fractional repulsive potential definition

Ge & Cui potential field definition (11) depends both on the distance ρ between the EGV and the obstacle, and their relative speed v_{RO}. Weyl potential field solely depends on the distance while distinguishing obstacle dangerousness with order n. Therefore, it is proposed to differentiate the obstacle dangerousness by keeping the order n in the Weyl repulsive field definition, and by adding distance and relative speed to add reactivity towards the obstacle. The new repulsive potential becomes:

$$U_{rep}(\boldsymbol{p}, \boldsymbol{v}) = \frac{\left(\rho_s(\boldsymbol{p}, \boldsymbol{p}_{obs}) - \rho_m(v_{RO})\right)^{n-2} - \rho_{max}^{n-2}}{\rho_{min}^{n-2} - \rho_{max}^{n-2}}, \quad (18)$$

from where one draws the repulsive force such as expressed in (14) with:

$$\nabla_p U_{rep}(\boldsymbol{p},\boldsymbol{v}) = \eta \frac{(n-2)\left(\rho_s\left(\boldsymbol{p},\boldsymbol{p}_{obs}\right)-\rho_m\left(v_{RO}\right)\right)^{n-3}\left(1+\frac{v_{RO}}{a_{max}}\right)}{\left(\rho_{min}^{n-2}-\rho_{max}^{n-2}\right)}\boldsymbol{n}_{RO} \tag{19}$$

and

$$\nabla_v U_{rep}(\boldsymbol{p},\boldsymbol{v}) = \eta \frac{(n-2)\left(\rho_s\left(\boldsymbol{p},\boldsymbol{p}_{obs}\right)-\rho_m\left(v_{RO}\right)\right)^{n-3} v_{RO}}{\rho_s\left(\boldsymbol{p},\boldsymbol{p}_{obs}\right) a_{max}\left(\rho_{min}^{n-2}-\rho_{max}^{n-2}\right)}\boldsymbol{v}_{RO\perp}\boldsymbol{n}_{RO\perp}. \tag{20}$$

Now, the repulsive potential field function takes into account an order n to avoid obstacles according to their dangerousness and the obstacle speed to operate in a dynamical environment.

4. SIMULATION EXAMPLE AND RESULTS

The proposed fractional repulsive potential field allows to take into account the dynamics of the obstacle as defined by Ge and Cui (2000) and Yin et al. (2009). However, it also takes into account the type of obstacle, previously indicated by Poty (2006) and Melchior et al. (2001). This field is indeed a combination of both methods. For the simulations, trajectory planning is seen as a control loop, such as illustrated in Figure 1

The controller used is in the form of a lead-phase controller as explained in section 2.

4.1 Study and scaling of factor η

Some research on potential fields suggests that a positive coefficient η applied to the repulsive force compensates for the magnitude of the attractive force. Usually, this factor η helps scaling the attractive and repulsive forces and is usually is defined empirically. Note that η is correlated to the ego vehicle mass. Here, a method to calculate the magnitude of this coefficient using the maximum value of the attractive force is proposed. Whatever the vehicle, there are dynamical acceleration and speed limits, among others. By knowing these limits, it is possible to define the maximum attractive force of the EGV:

$$\max(F_{att}) = F_{att}^{max} = m_{ego} a_{max}, \tag{21}$$

where m_{ego} represents the mass of the ego-vehicle, and a_{max} represents its maximum acceleration. This maximum force already gives us a magnitude order of the force exerted on the vehicle. Note that the repulsive force must be greater than the attractive force, in order to avoid a collision. To achieve this goal, η is defined by F_{att}^{max} to a factor k, such as:

$$\eta = k F_{att}^{max}. \tag{22}$$

So-defined, η becomes is dependent of the vehicle mass.

Figure 4 presents the results obtained with different values of k. ρ_{min} is fixed to the radius of the obstacle or the minimum acceptable distance between the ego-vehicle and the obstacle, and $\rho_{max} = 2\rho_{min}$. When the obstacle is practically aligned with the ego-vehicle and the target, it is indeed one of the worst cases as the ego-vehicle may be trapped in a local minima.

The coefficient k depends on the type of obstacle. In the case of a square obstacle, it is necessary that the repulsive force be greater because of the presence of corners.

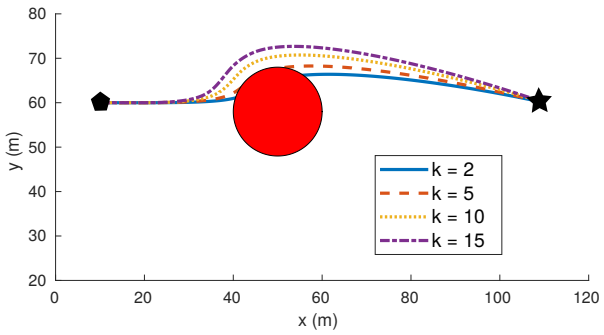

Fig. 4. Robot path with a round obstacle for different k : $\eta = kF_{att}^{max}$; $m_{ego} = 1.5kg$

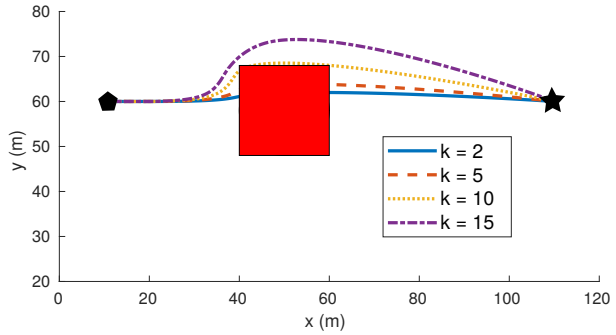

Fig. 5. Robot path with a square obstacle for different k : $\eta = kF_{att}^{max}$; $m_{ego} = 1.5kg$

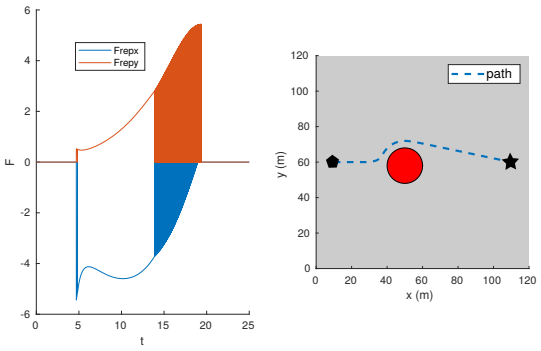

Fig. 6. Robot path with a round obstacle and a factor $k = 15$: $\eta = kF_{att}^{max}$; $m_{ego} = 1.5kg$

One of the outcomes of this study lies in the fact that the coefficient η no longer depends on the mass of the ego-vehicle, such as illustrated on Figure 6 and Figure 7. It is the type of the obstacle that impacts the value of this coefficient. Indeed, the path is no more affected by the mass variations as only the force values are modified. To conclude, fixing k to 15 enables avoiding any kind of obstacle shape.

4.2 Simulation results in a 3D dynamical environment

In the simulation scenario, there are one static target, two static obstacles (sphere) and one dynamical obstacle

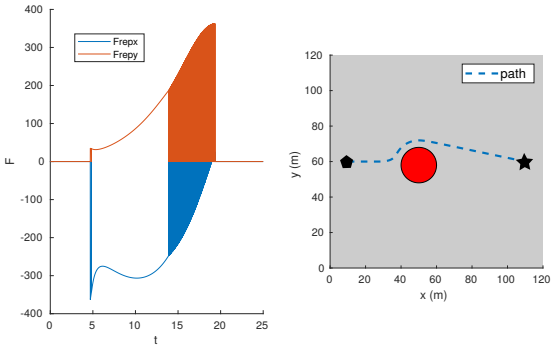

Fig. 7. Robot path with a square obstacle and a factor $k = 15 : \eta = kF_{max}$; $m_{ego} = 100kg$

(cube). Table 1 summarizes the initial conditions of each element. Figure 8 represents the 3D environment map. Three methods are compared: the Ge & Cui repulsive potential, the Weyl fractional repulsive one and the dynamical fractional repulsive one. The parameters concerning the attractive forces Ge and Cui are given in section 2.1. The parameters concerning the repulsive forces are shown in Table 2. The mass of the EGV is $m = 1.5kg$ which corresponds to the mass of an Iris + drone.

Table 1: Initial conditions

Element	Position	Velocity
EGV	$[0, 0, 10]$	$[0, 0, 0]$
Obstacle 1	$[20, 25, 10]$	$[0, 0, 0]$
Obstacle 2	$[90, 95, 10]$	$[0, 0, 0]$
Obstacle 3	$[70, 70, 10]$	$[0, 0, -1]$
Target	$[120, 120, 10]$	$[0, 0, 0]$

Table 2: Repulsive potential parameters

Element	Method	k	n	shape
Obstacle 1	Ge & Cui	150	-	sphere
	Weyl potential	10	0.5	
	dynamical fractional	10	0.5	
Obstacle 2	Ge & Cui	150	-	sphere
	Weyl potential	10	0.5	
	dynamical fractional	10	0.5	
Obstacle 3	Ge & Cui	200	-	cube
	Weyl potential	15	0.5	
	dynamical fractional	15	0.5	

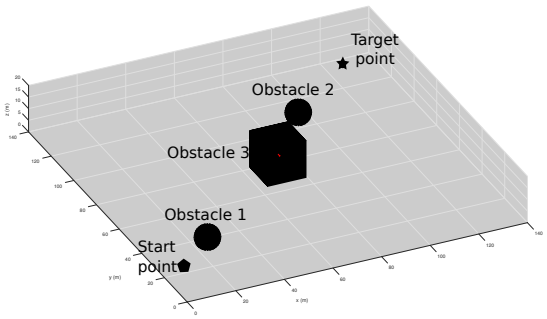

Fig. 8. 3D Environment Map

Figure 9a shows the trajectories using three different methods, Weyl potential (green), Ge & Cui (red), dynamical

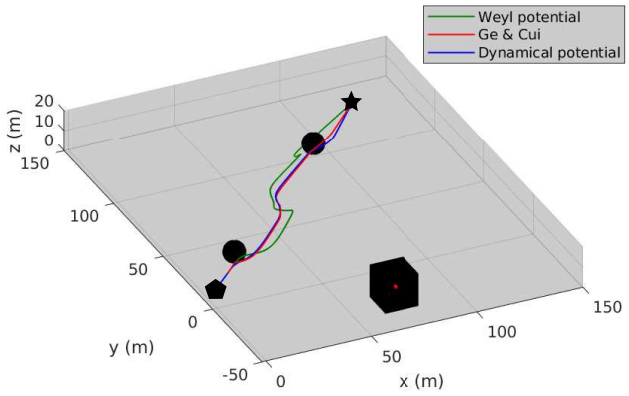

(a) Whole simulation

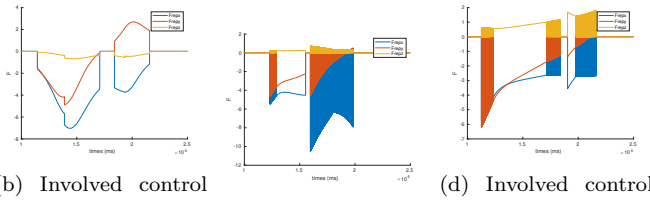

(b) Involved control repulsives forces for Weyl potential method

(c) Involved control repulsives forces for Ge & Cui method

(d) Involved control repulsives forces for dynamical potential method

Fig. 9. Path and forces obtained with the three methods

potential (blue). As obstacles 1 and 2 are static, let us focus on the dynamical obstacle 3. In Ge & Cui method, as this field takes into account the dynamical aspect of the obstacle, the ego-vehicle avoids obstacle 3 in the opposite direction of the obstacle speed. In Weyl Fractional repulsive potential, as the obstacle speed is not considered, the avoidance of obstacle 3 takes more time as the EGV is forced to travel more distance, and is undertaken on the other way around. In the proposed dynamical fractional repulsive potential, the trajectory is very close to that of Ge & Cui. This method takes into account the dynamical aspect of the obstacles and furthermore, it is possible to adjust the level of danger n of the obstacles.

Figure 10 is the same scenario as in Figure 9 and represents the trajectory with an order n of the cube obstacle varying from 0.2 to 1.5. To better visualize the influence of the degree n, only a zoom of the trajectory around the cube obstacle has been shown. Note that the higher the order, the sooner the avoidance of the obstacle. The trajectory is also smoother, but having a lower order enables going nearer to the obstacle and having a shorter trajectory. The key is to find a compromise between getting closer to the obstacle in a safe manner and travelling the shortest the distance.

Table 3 summarizes the results: the higher the obstacle danger degree n, the sooner the obstacle avoidance, and therefore the safer the trajectory, however, the farther the trip distance and the higher the energy consumption.

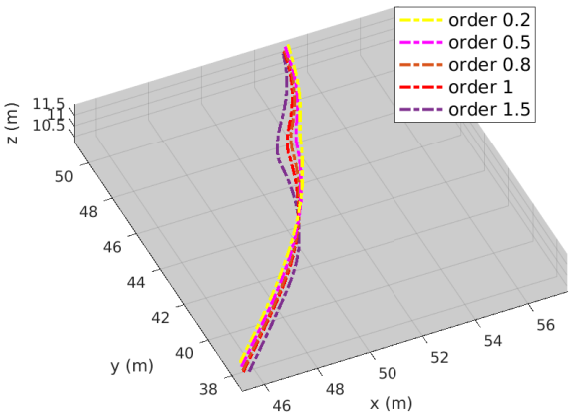

Fig. 10. Robot path with dynamical fractional repulsive force and n varying from 0.2 to 1.5

5. CONCLUSION

Artificial potential fields provide good results for trajectory planning in dynamical environments. It remains essential for real-time applications and allows a good reactivity of the EGV. The Ge & Cui repulsive force solely allows taking into account the velocity of obstacles without considering their dangerousness. Moreover, the Weyl potential force associates a degree of danger with an obstacle but do not consider the obstacle dynamics. On the contrary, the proposed new dynamical fractional repulsive field presents both advantages. Our method takes into account the obstacle dynamics, such as positions and speeds, and associates dangerousness with a fractional degree. For future works, it would be interesting to consider a fractional controller in the attractive PF, so that robustness in terms of EGV mass variations and disturbance rejection is guaranteed. In addition, a complete UAV model could be considered instead of a mass point model.

Table 3: Comparative study

method	n	time (s)	length (m)	energy (J)
Ge & Cui	/	74.45	176.73	$1.325.10^3$
Weyl potential	1.5	79.99	189.81	$1.424.10^3$
dyn. frac. pot.	0.2	71.67	174.94	$1.312.10^3$
dyn. frac. pot.	0.5	72.35	175.36	$1.315.10^3$
dyn. frac. pot.	0.8	72.93	175.69	$1.318.10^3$
dyn. frac. pot.	1	73.25	175.85	$1.319.10^3$
dyn. frac. pot.	1.5	73.71	176.21	$1.322.10^3$

REFERENCES

Ge, S. and Cui, Y. (2000). New potential functions for mobile robot path planning. *IEEE Transactions on Robotics and Automation*, 16(5), 615–620. doi: 10.1109/70.880813.

Ge, S. and Cui, Y. (2002). Dynamic motion planning for mobile robots using potential field method. *Autonomous Robots*, 13(3), 207–222. doi:10.1023/A:1020564024509.

Khatib, O. (1985). Real-time obstacle avoidance for manipulators and mobile robots. In *Proceedings. 1985 IEEE International Conference on Robotics and Automation*, volume 2, 500–505. doi: 10.1109/ROBOT.1985.1087247.

Krogh, B. and Thorpe, C. (1986). Integrated path planning and dynamic steering control for autonomous vehicles. In *Proceedings. 1986 IEEE International Conference on Robotics and Automation*, volume 3, 1664–1669. doi:10.1109/ROBOT.1986.1087444.

Li, G., Tong, S., Cong, F., Yamashita, A., and Asama, H. (2015). Improved artificial potential field-based simultaneous forward search method for robot path planning in complex environment. In *2015 IEEE/SICE International Symposium on System Integration (SII)*, 760–765. doi:10.1109/SII.2015.7405075.

Mac, T.T., Copot, C., Hernandez, A., and De Keyser, R. (2016). Improved potential field method for unknown obstacle avoidance using uav in indoor environment. In *2016 IEEE 14th International Symposium on Applied Machine Intelligence and Informatics (SAMI)*, 345–350. doi:10.1109/SAMI.2016.7423032.

Melchior, P., Irnan, C., Metoui, B., and Oustaloup, A. (2012). Robust path planning for mobile robot based on fractional attractive force in 3-dimension space. *IFAC Proceedings Volumes*, 45(2), 577 – 582. doi: 10.3182/20120215-3-AT-3016.00102. 7th Vienna International Conference on Mathematical Modelling.

Melchior, P., Orsoni, B., and Oustaloup, A. (2001). Weyl fractional potential in path planning. In *6th European Control Conference ECC'01*. Porto, Portugal. doi: 10.23919/ECC.2001.7076175.

Metoui, B., Melchior, P., Najar, S., Abdelkrim, M.N., and Oustaloup, A. (2009). Robust path planning for dynamic environment based on fractional attractive force. In *2009 6th International Multi-Conference on Systems, Signals and Devices*, 1–8. doi: 10.1109/SSD.2009.4956793.

Poty, A. (2006). *Planification de Trajectoire dans un Environnement Dynamique et Génération de Mouvement d'Ordre Non Entier*. Ph.D. thesis, Université Bordeaux 1, France.

Poty, A., Melchior, P., and Oustaloup, A. (2004). Dynamic path planning for mobile robots using fractional potential field. In *First International Symposium on Control, Communications and Signal Processing, 2004.*, 557–561. doi:10.1109/ISCCSP.2004.1296443.

Receveur, J., Victor, S., and Melchior, P. (2019). New interpretation of fractional potential fields for robust path planning. *Fractional Calculus & applied analysis*, 22(1), 113–127. doi:10.1515/fca-2019-0007.

Sfeir, J., Saad, M., and Saliah-Hassane, H. (2011). An improved artificial potential field approach to real-time mobile robot path planning in an unknown environment. In *2011 IEEE International Symposium on Robotic and Sensors Environments (ROSE)*, 208–213. doi:10.1109/ROSE.2011.6058518.

Yin, L., Yin, Y., and Lin, C. (2009). A new potential field method for mobile robot path planning in the dynamic environments. *Asian Journal of Control*, 11(2), 214–225. doi:10.1002/asjc.98.